XX Fluid Mechanics Conference KKMP2012,
Gliwice, 17-20 September 2012

LOCAL PARAMETERS OF THE LIQUID AT THE OUTLET OF THE FORMED SUCTION INTAKE OF VERTICAL AXIAL-FLOW PUMPS

Andrzej Błaszczyk [1], Radosław Kunicki [1], Adam Papierski [1]
Institute of Turbomachinery Technical University of Lodz, Poland;
E-mail: adam.papierski@p.lodz.pl

Key words: suction intake, unsteady flow, model studies

Abstract:

There are introduced results of numerical computations and Pitot probe measurements of velocities at the outlet of the formed suction intake, with and without the rib. There are given conclusions of the comparative analysis of numerical computations and Pitot probe measurements. These results may constitute the basis of verification of the unsteady flow computation method, for formed suction intakes, proposed in the thesis [8].

1. INTRODUCTION

Formed suction intake is the final element of water intake system of mixed flow or vertical axial-flow pumps. In the Fig. 1 there is shown the scheme of the analyzed inlet channels system of the analyzed facility.

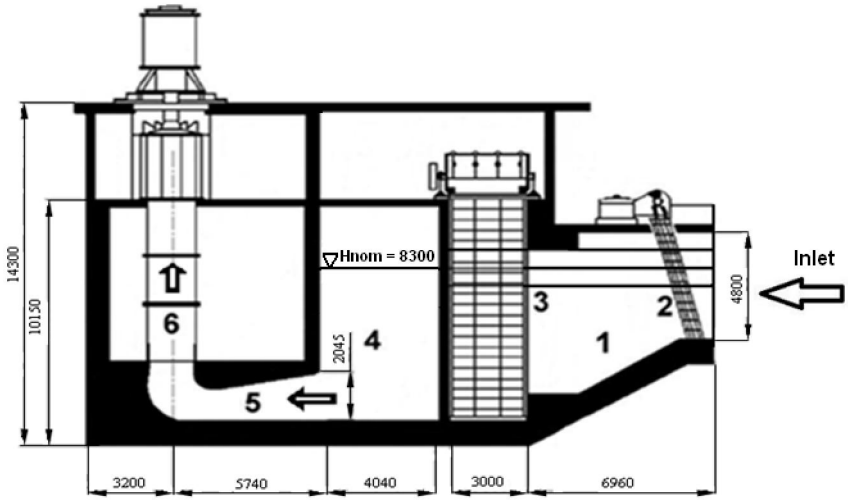

1-screen chamber, 2-trash screens, 3-rotary screen, 4-open wet well,
5-formed suction intake, 6-outlet pipe,

Fig. 1. The real facility – system of the open wet well [8]

In the scheme above there are marked characteristic dimensions of the pumping system and the nominal water level at the intake $H_n = 8300\ mm$. Due to the construction and casing of the pumping system, flow parameters measurements are not carried out in the real facility.

At the pumping facility design stage, measurements and observations of a flow in a water pumping system are carried out using a model of the real facility.

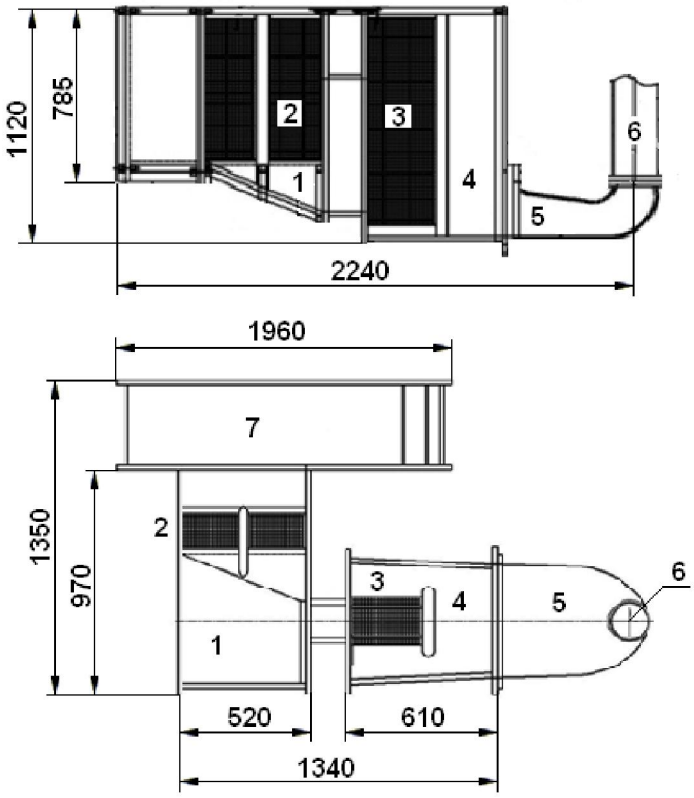

1-screen chamber, 2-trash screens, 3-rotary screen, 4-open wet well, 5-formed suction intake, 6-outlet pipe,7- delivery channel

Fig. 1. Scheme of the water pumping system, open wet well and the suction intake [3, 4]

Model was made in 1:10 scale. The model consists of: the screen chamber (1), trash screens (2), rotary screen (3), open wet well (4), formed suction intake (5), outlet pipe (6), delivery channel – the high-water source model (7).

Due to the change of the flow direction from horizontal to vertical, in the formed suction intake, the unsteady flow phenomena are induced.

Unsteady flow parameters (pressure and velocity)of the water flowing out from the formed suction intake have a decisive influence on the pump impeller operation, frequently causing changes in its' efficiency.

Uncontrolled changes in the cooling water pump efficiency may be the cause of power fluctuations in the power unit, which are highly adverse for the operation of the turbine set.

Disposal of unfavorable hydraulic phenomena requires most of all their identification.

Up to now, parameter measurements of the liquid flow (pressures, velocities) and observations of swirl structures in the flowing water, were impossible in flow channels made of an organic glass in the 1:10 and 1:20 scale.

Nowadays it can be observed in the available literature [5, 6, 9, 10, 11, 12, 13] the trend of replacing the expensive model studies for computing flows with numerical computation methods for fluid dynamics.

Numerical computations may be used to:

- develop coherent inlet chamber and intake design methods,
- reduce costs of designing inlet chambers and intakes by eliminating expensive model studies.

In following chapters there is introduced the numerical computation method for computing velocities, which mean values are compared to velocities measured on the test stand. The results of comparisons of average speed of calculations and measurements were the basis for the decision on the application of the proposed method, numerical calculations of transient flows.
Comparative analysis was carried out for two variants of the suction intake, without and with the rib. (Fig. 3, Fig. 4)

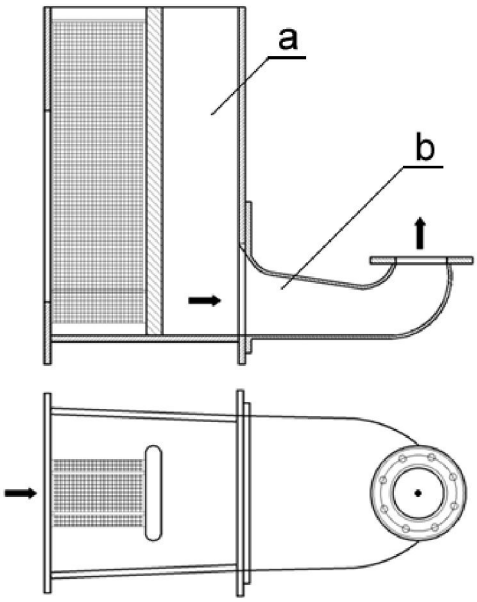

a- open wet well, b- formed suction intake

Fig. 3. Model of the open wet well and the suction – without the rib

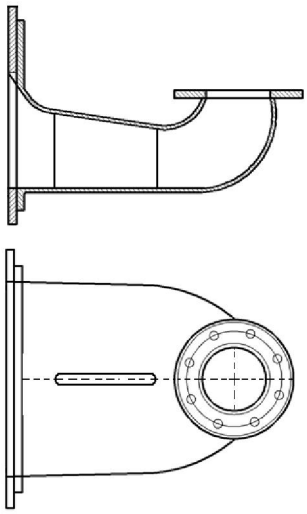

Fig. 4. Model of the formed suction intake with the rib

2. Flow numerical computation method

On the basis of initial velocity computations, which results were compared to measured velocities, there was engaged the ANSYS CFX software with the turbulence model SST.

2.1.Numerical computations procedure

Scheme of the algorithm of the applied method for numerical computations of unsteady flows, shown in the Fig. 5.

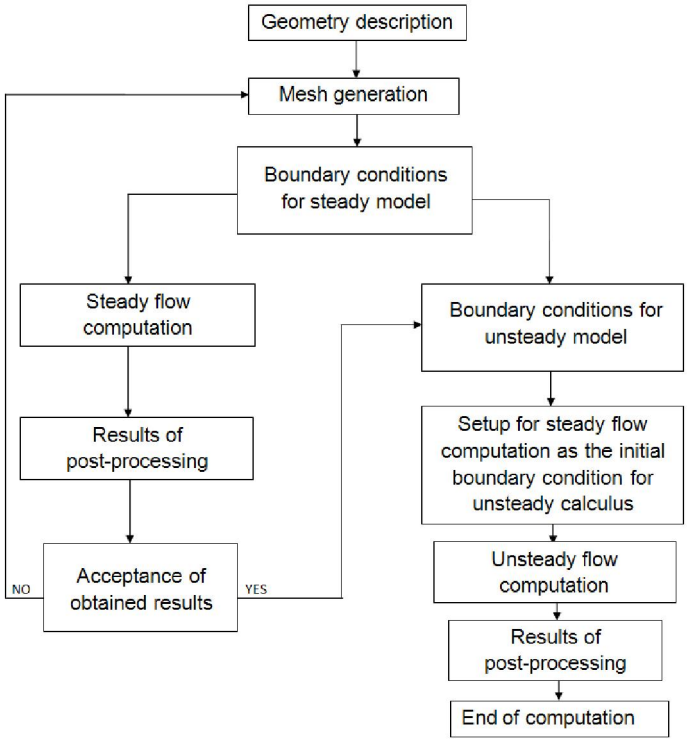

Fig. 5. Scheme of the algorithm of the method for unsteady flows computations

2.2.Required numerical parameters and boundary conditions

Required numerical parameters were explained below in order to authenticate results of computations.

Generated mesh was evaluated (for acceptance) according to the following criteria:

- number of nodes is 2.5 million,
- number of control volumes for the suction intake construction with and without the rib is 3.6 million,
- ratio of the longest to the shortest side of the control volume (Aspect Ratio): 1 – 100,
- skewness of the mesh corresponds to the angle between two adjoining planes in the control volume: 0 – 0,95 - according to the formula:

$$Skewness = \max\left[\frac{\theta_e - \theta_{\min}}{\theta_e}\right] \qquad (2.1)$$

where:

$\theta_e = 60° \; or \; 90°$ depending on the computing mesh type,
$\theta_{\min}$ – minimal skewness angle of the mesh,

- ratio of the contacting the highest and the lowest volume of the mesh (Expansion Factor: recommended < 20.

In following figures there are shown the geometry and computing mesh for the suction intake without the rib (Fig. 6) and for the suction intake with the rib (Fig. 7).

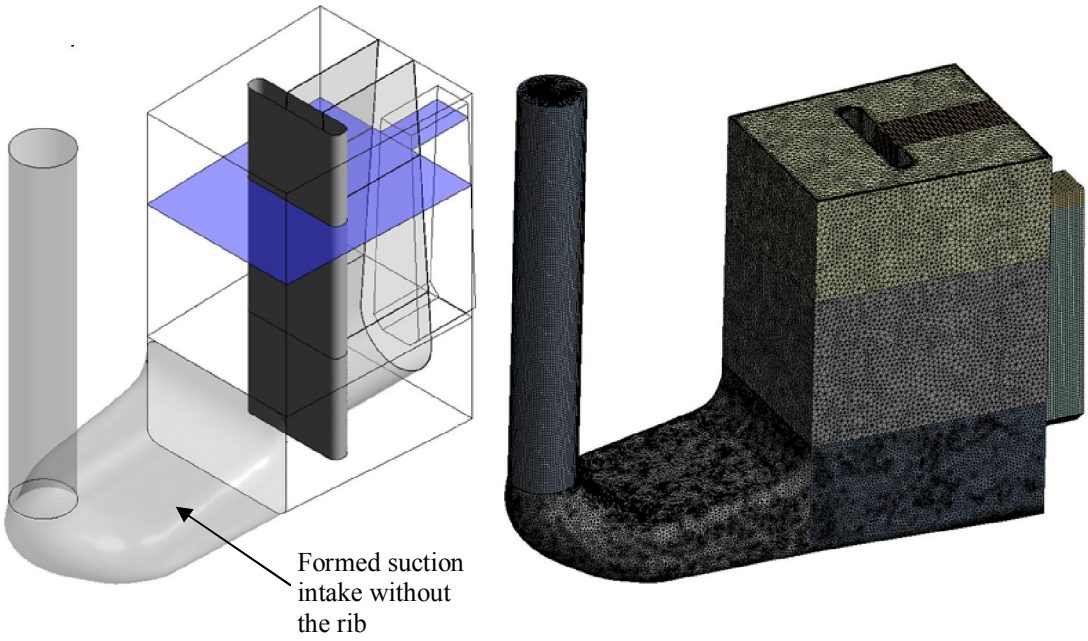

Fig. 6. Geometry and the computing mesh of the suction intake without the rib

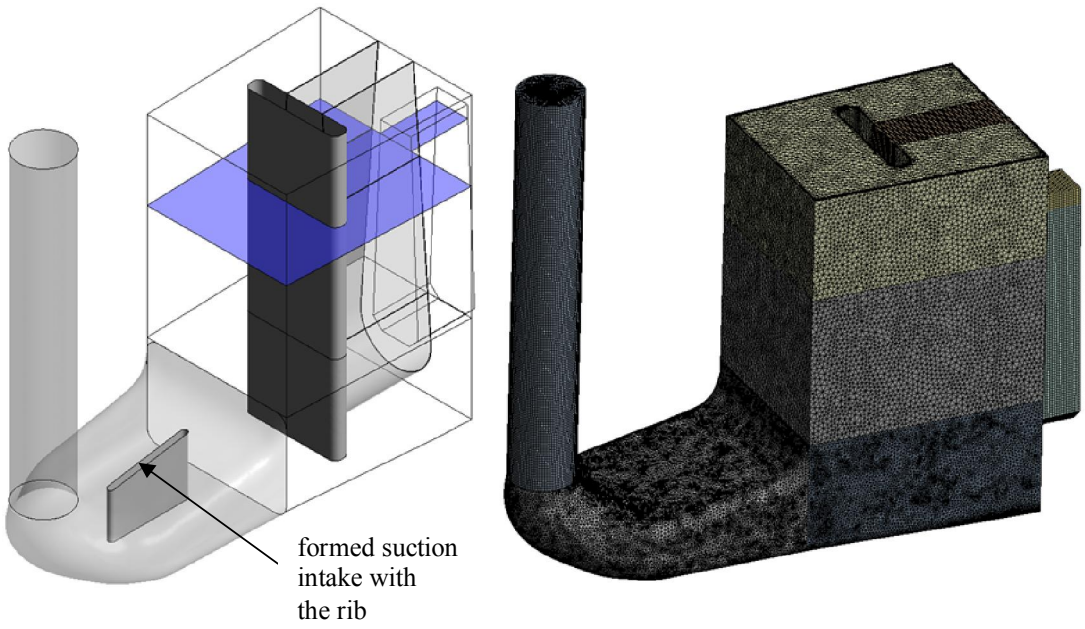

Fig. 7. Geometry and the computing mesh of the suction intake with the rib

There were assumed following boundary conditions:

- total pressures at the inlet of the suction intake defined by the formula (2.2).

$$p = \rho g H + \frac{\rho \left(\frac{Q}{A_ł}\right)^2}{2} \tag{2.2}$$

where:

H – height of the water collumn in the suction intake model,
ρ – density of the water,
$A_ł$ – surface area of the screen chamber to the open wet well connector,
Q – efficiency of the liquid flowing through the open wet well.

- creation of the free liquid surface according to the Fig. 8,

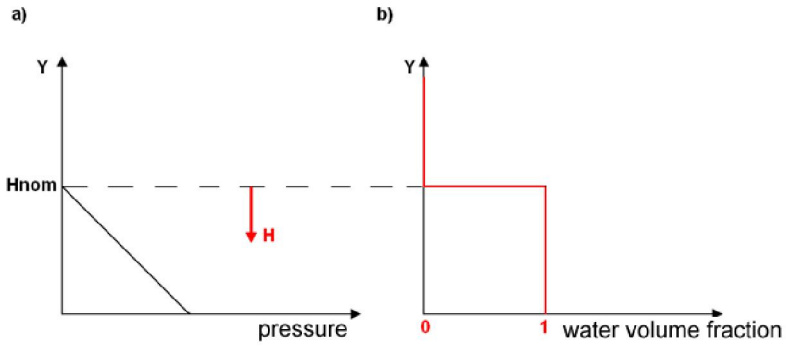

Fig. 8. Conditions for creation of the free liquid surface at the inlet to the computing zone of the open wet well:
a) hydrostatic pressure b) volume fraction of the water

- the turbulence intensity at the level of 5% (when $I = 10$) according to the formula:

$$I = \frac{\mu_t}{\mu_d} \tag{2.3}$$

where: μ_t – turbulent viscosity,
μ_d – dynamic viscosity

- mass flow at the outlet of the suction intake: $\dot{m} = 24{,}6\ \mathrm{kg/s}$,
- zero gradient of the pressure in the main flow direction (this condition is assumed internally by the ANSYS-CFX preprocessor)

Computations required additional settings:

- active surface area of the rotary screen to the whole surface ratio (Volume Porosity): 74%
- assumptions of the porous surface at the rotary screen, causing the pressure loss at the screen of $\Delta p = 60\ Pa$,
- screen resistance coefficient (Quadratic resistance coefficient) using the formula:

$$K_Q = \left(\frac{\Delta p}{\Delta x}\right) {c_{por}}^2 \tag{2.4}$$

where:

Δp –pressure loss at the porous surface
Δx – thickness of the porous surface

c_{por} – velocity of the agent through the porous surface

- assumption of walls hydraulically smooth,
- assumption of the logarythmic distribution of the velocity at the wall, the so called Wall Function. In the Fig.10 there is shown the diagram of dimensionless velocity u+ in the function of the dimensionless distance from the wall y+. In order to have the Function Wall working properly, the first node of the mesh must be located in the distance not less than y+=12 and not further then y+=200 (Fig. 11). For values y+<11 the mesh node is in the laminar sub-layer, and for y+>300 beyond the boundary layer. Initial computations reveal that the maximal value y+= 150.

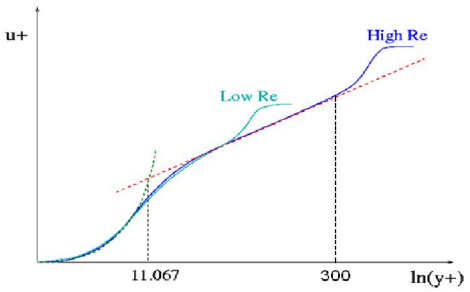

Fig. 9. Scope of values of y+ [8]

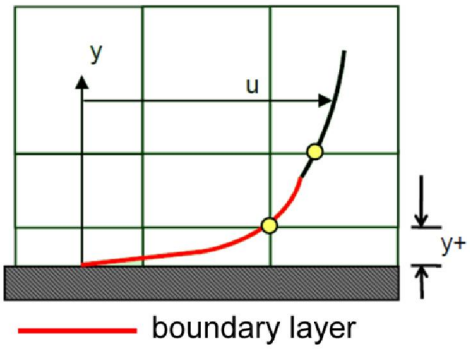

Fig. 2. Orientation of the first mesh node in the boundary layer in the logarithmic velocity distribution zone (boundary layer) [8]

Values of the dimensionless distance y+ for the geometry mesh (example) are shown in the Fig. 11.

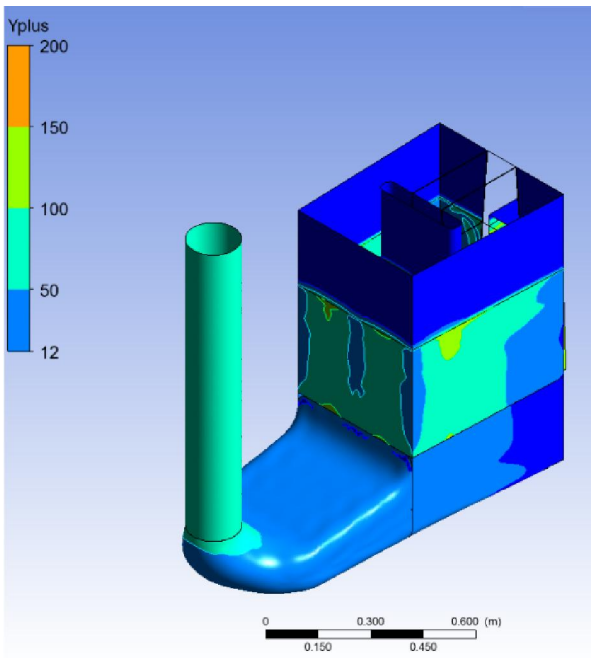

Fig. 11. Values of y+ for the geometry mesh

- the Courant number – is the basic criterion in computations of unsteady flows defined as:

$$Courant = \frac{u\Delta t}{\Delta x} \tag{2.5}$$

where:

u – agent velocity,
Δt – time step,
Δx – size of the mesh node.

Scope of the Courant number values in use of the turbulence model SST is not formulated. It is recommended to assume such value, that it enables to obtain the problem solution in the assumed residuum level [2]. In considered models of the open wet well and suction inlet , the value of the Courant number varied in the scope of $(0{,}08 \div 2{,}04)$. For this value it was obtained the assumed residuum level,

- time of the complete computation: 30 [s],
- time step in computations: 0,001 [s],
- minimal number of iterations for the given time step: 1,
- maximal number of iterations for the given time step:12,
- discretisation level of the convection member of the II order,
- time step of the solution recording: 0,05 [s].

3. The test stand

Design of the water pumping system model was made out of condition of the Froude number equality in the intake cross-section for the facility and model.
The measuring equipment of the test stand enabled measurements of values slowly varying in the time constant of few seconds, which mean values were used to verify results of numerical computations.

3.1.Test stand structure

Basic elements of the test stand are:
water container, installation piping system with control valves and the equalizing tank, circulation pump forcing the flow and the pumping system model.
Pumping system model was composed of:

- runner,
- screen chamber,
- inlet channels to the intake,
- rotary screen,
- open wet well and the suction intake of the pump finished in the position of its' installation with the outlet pimping section.

Test stand was shown in the Fig. 13.

a)

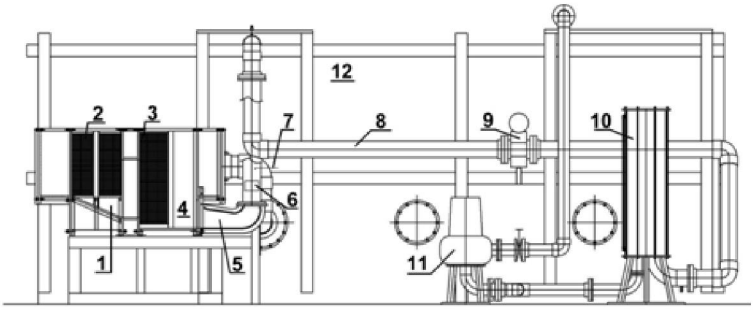

b)

c)

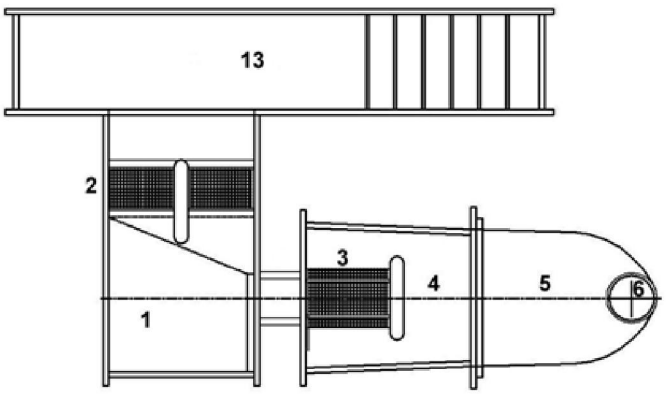

Fig. 3 Experimental test stand [3]:

a) test stand scheme, b) stand facade, c) water pumping system (top view)
1) screen chamber, 2) trash screens, 3) rotary screen, 4) open wet well,
5) formed suction intake, 6) swirl-meter, 7) Pitot probe, 8) piping, 9) flow-meter, 10) equalizing tank,
11) circulating pump, 12) main water container,
13) runner – model of the high-water source.

3.2.Measuring instrumentation of the formed suction intake outlet

In the Fig. 13 and Fig. 14 there are introduced elements of the instrumentation for the velocity measurements (at the outlet of the suction intake).

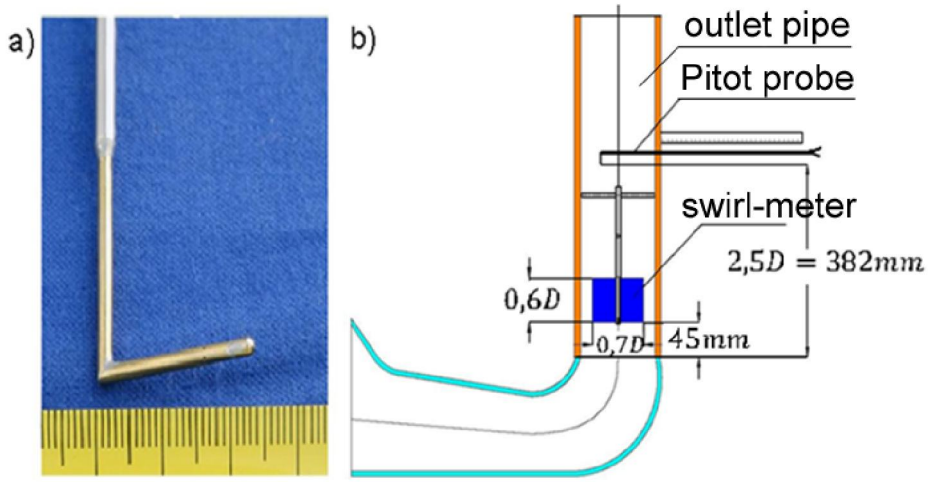

Fig. 13. Scheme of the Pitot probe installation and the swirl-meter in the outlet pipe a) view of the probe b) view of the swirl-meter

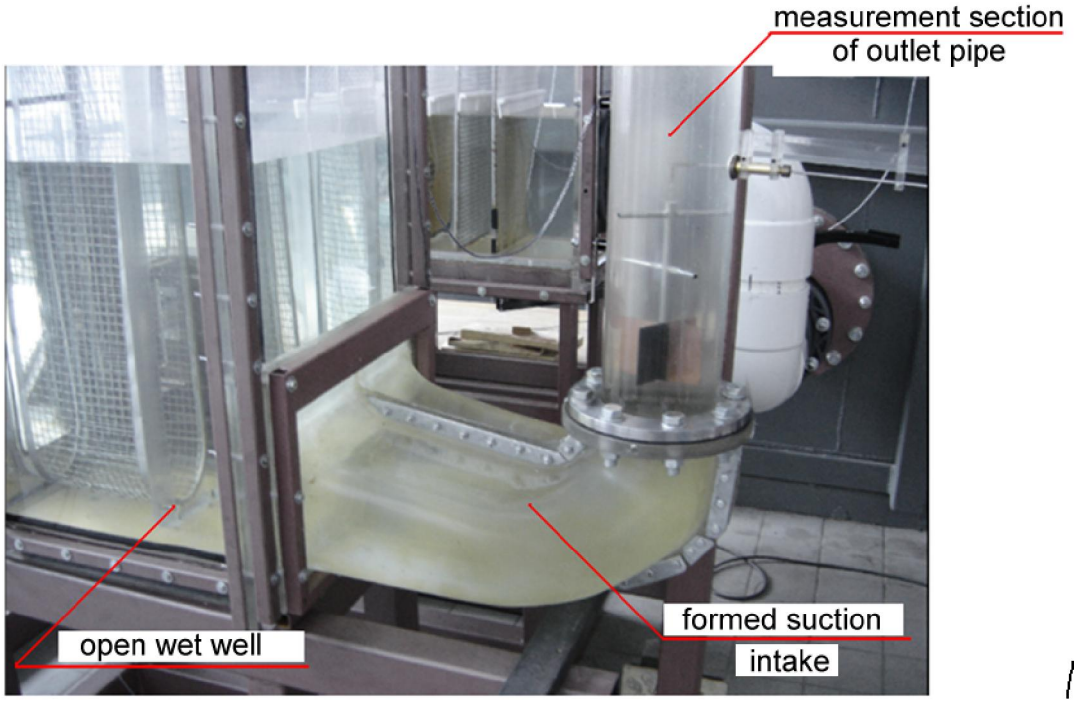

Fig. 14 View of the suction intake , the open wet well and the suction piping (outlet pipe) with the installed Pitot probe and the swirl-meter [3, 4]

Measurements of the velocity using the Pitot probe, in the case of the suction intake without the rib, were carried out in points shown in the Fig. 15.

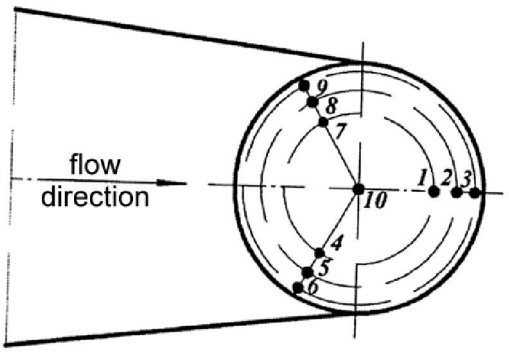

Fig. 4. Measurement points using the Pitot probe for the suction intake without the rib [3,4]

Whereas, for the suction intake with the rib measurements were carried out in points shown in the Fig. 16.

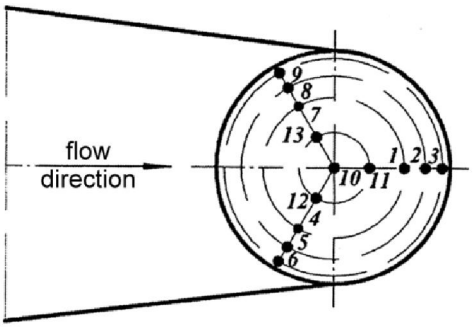

Fig. 16. Measurement points using the Pitot probe for the suction intake with the rib [3,4]

4. Velocities at the outlet from the formed suction intake

In the chapter 4.1, 4.2 were introduced for the each measurement point diagrams of velocities from numerical computations and the measurement using the Pitot probe. These diagrams were used in the comparative analysis and in the liquid flow evaluation in the aspect of meeting the criteria required in the standard [1]:

- velocity fluctuations in time in the given point of the probe measurement,
- non-uniformities of the velocity profile.

4.1. Velocities from numerical computations and measurements for the suction intake without the rib

Graphic illustration of variations in time of numerically computed velocities and measurements and measurements for the suction intake without the rib were shown in figures 17a - 26a and 17b - 26b.

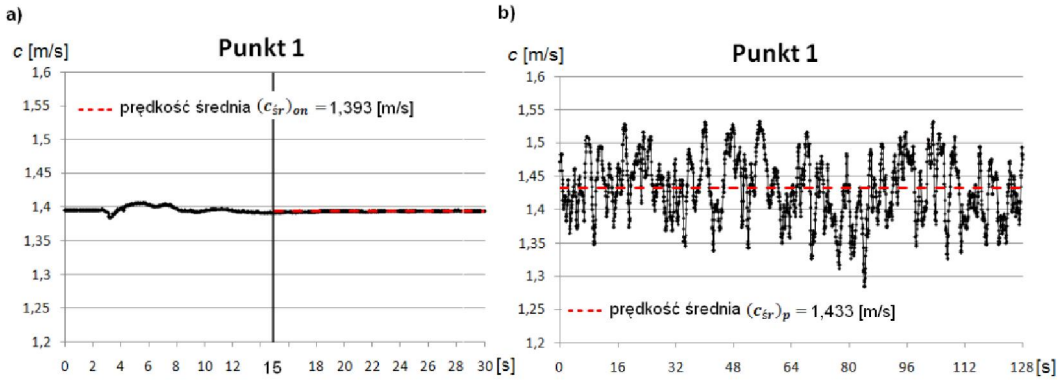

Fig. 17. Time variations of the velocity for the measurement point of the probe 1: a) computed numerically b) using the Pitot probe

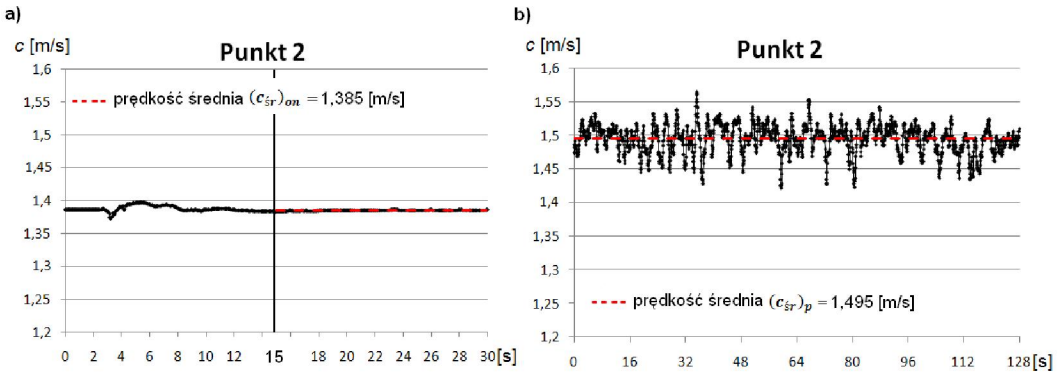

Fig.18. Time variations of the velocity for the measurement point of the probe 2: a) computed numerically b) using the Pitot probe

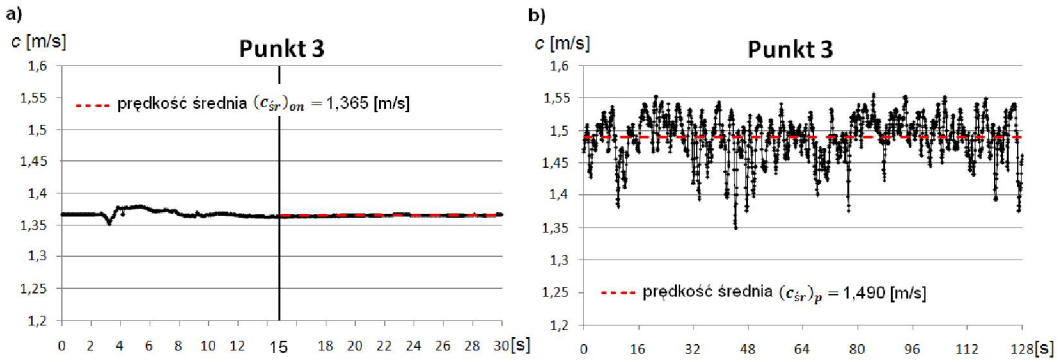

Fig.19. Time variations of the velocity for the measurement point of the probe 3: a) computed numerically b) using the Pitot probe

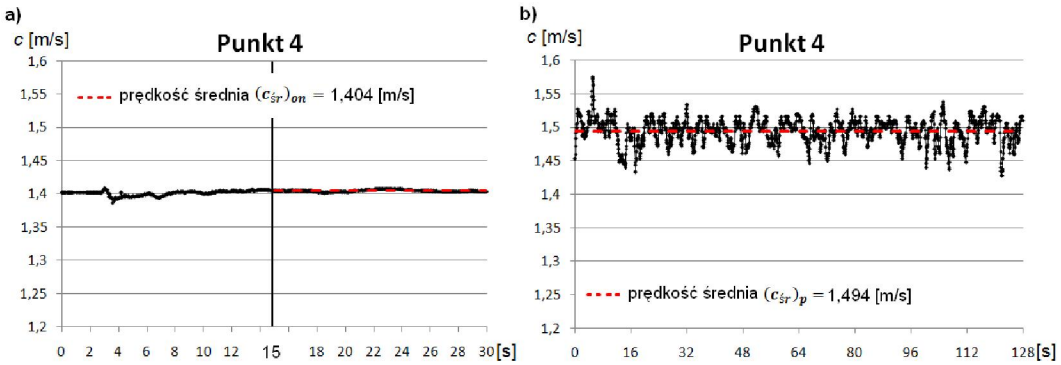

Fig.20. Time variations of the velocity for the measurement point of the probe 4: a) computed numerically b) using the Pitot probe

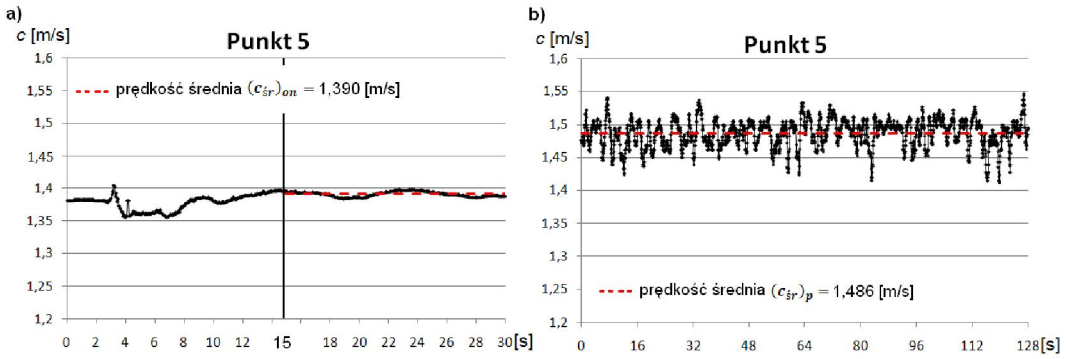

Fig. 21.Time variations of the velocity for the measurement point of the probe 5: a) computed numerically b) using the Pitot probe

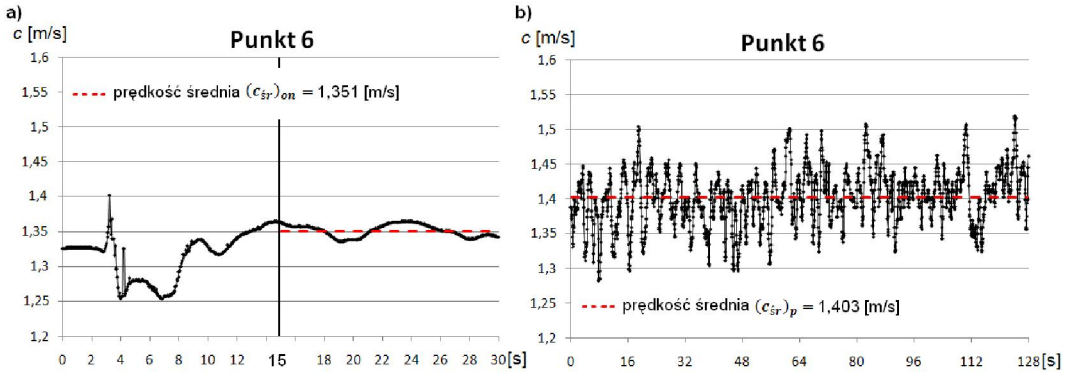

Fig.22. Time variations of the velocity for the measurement point of the probe 6: a) computed numerically b) using the Pitot probe

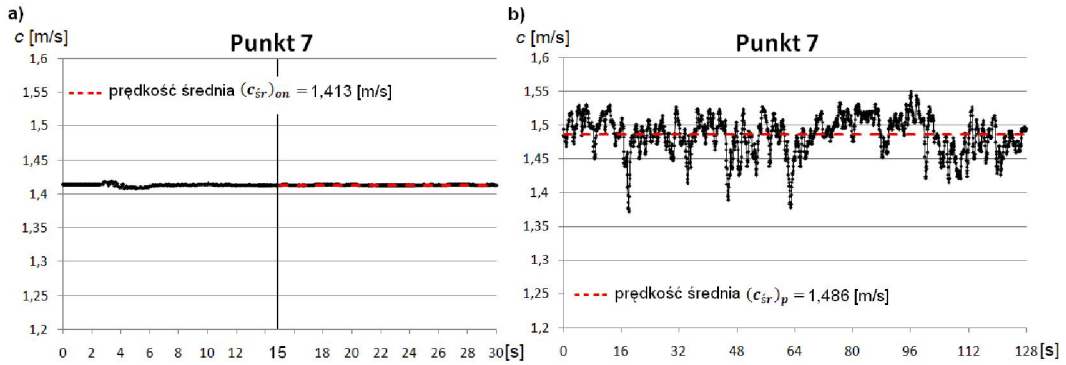

Fig. 53 Time variations of the velocity for the measurement point of the probe 7: a) computed numerically b) using the Pitot probe

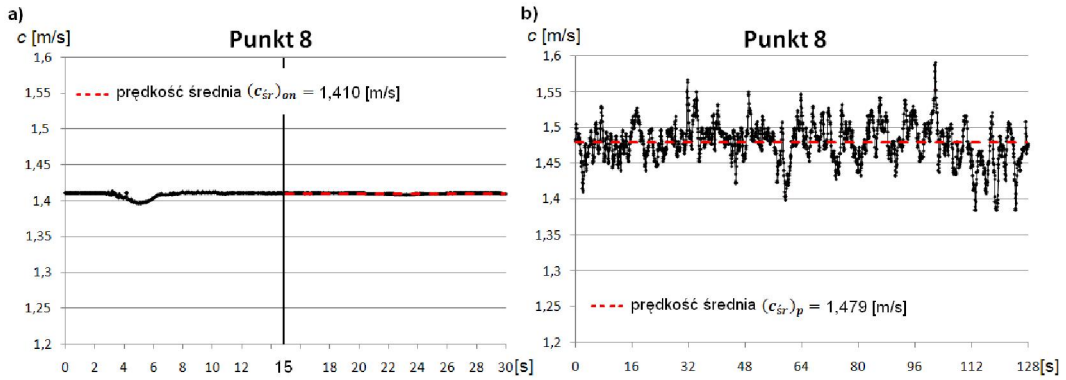

FIg.24. Time variations of the velocity for the measurement point of the probe 8: a) computed numerically b) using the Pitot probe

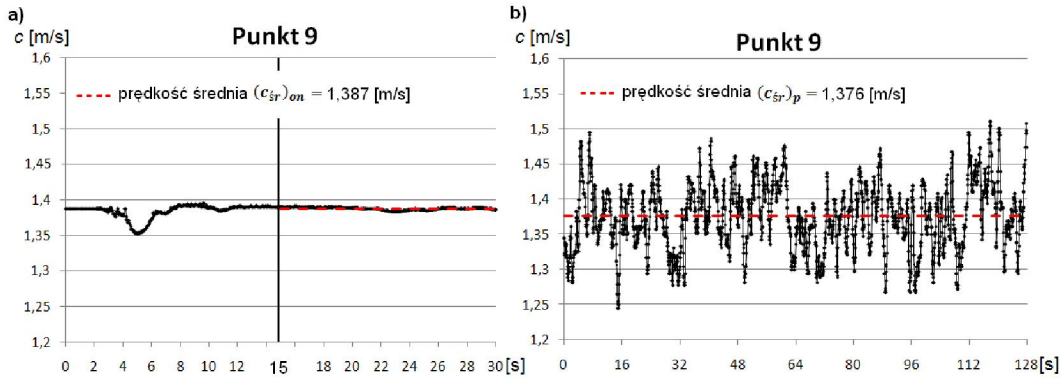

Fig.25. Time variations of the velocity for the measurement point of the probe 9: a) computed numerically b) measuring the Pitot probe

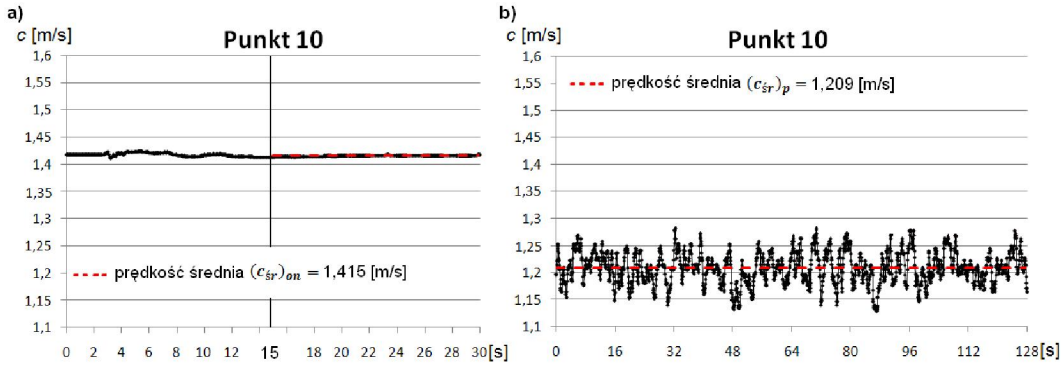

FIg. 26 Time variations of the velocity for the measurement point of the probe 10: a) computed numerically b) measuring the Pitot probe

In these pictures were marked mean values of the velocity form numerical computations $(c_{śr})_{on}$ and measurements $(c_{śr})_p$ using lines.

4.2.Velocities from numerical computations and measurements for the suction intake with the rib

Graphical illustration of time varying velocities from numerical computations and measurements for the suction intake with the rib were shown in 27a – 39a and 27b – 39b.

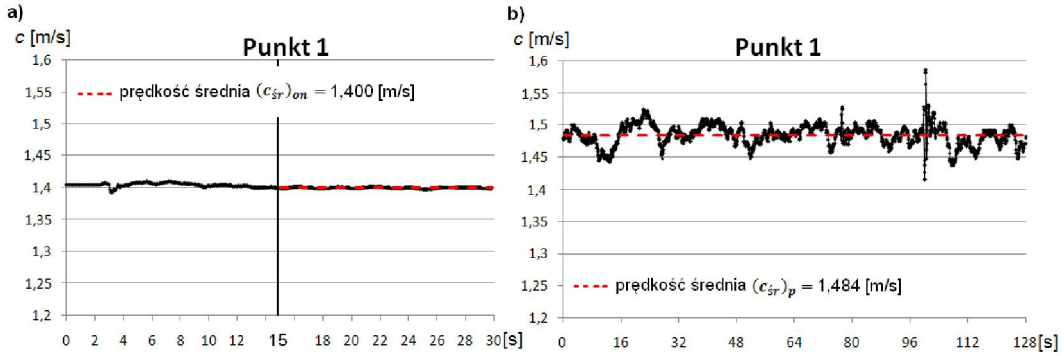

Fig.27. Time variations of the velocity for the measurement point of the probe 1: a) computed numerically b) measuring the Pitot probe

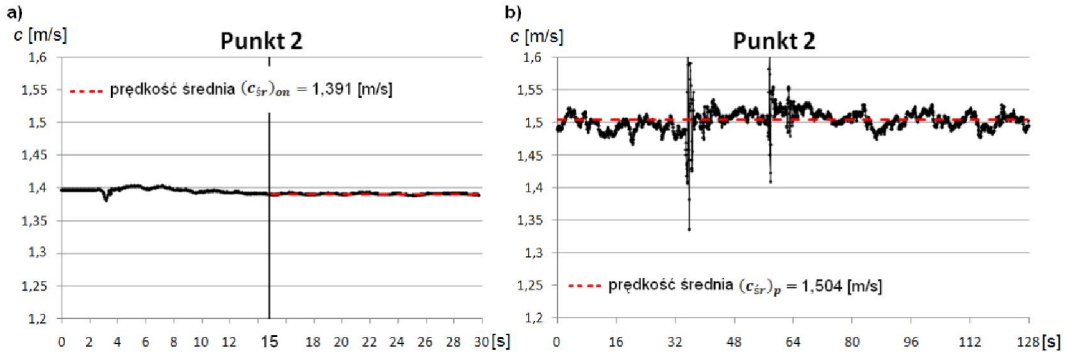

Fig.28. Time variations of the velocity for the measurement point of the probe 2: a) computed numerically b) measuring the Pitot probe

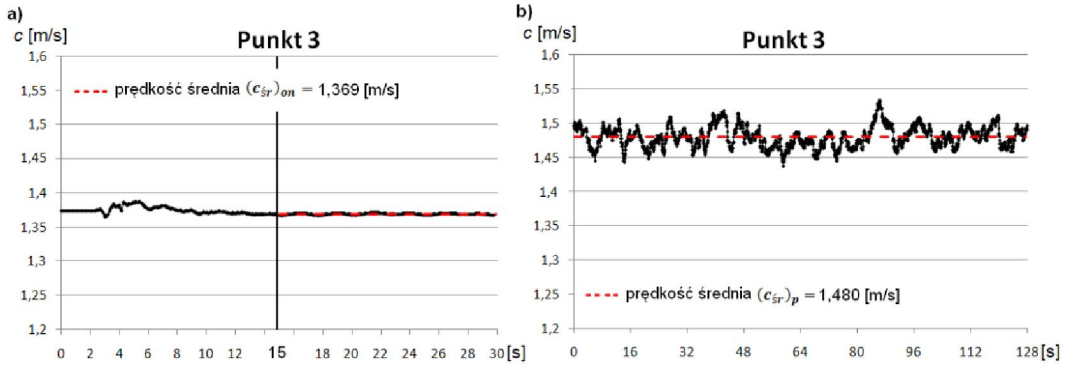

Fig. 29. Time variations of the velocity for the measurement point of the probe 3: a) computed numerically b) measuring the Pitot probe

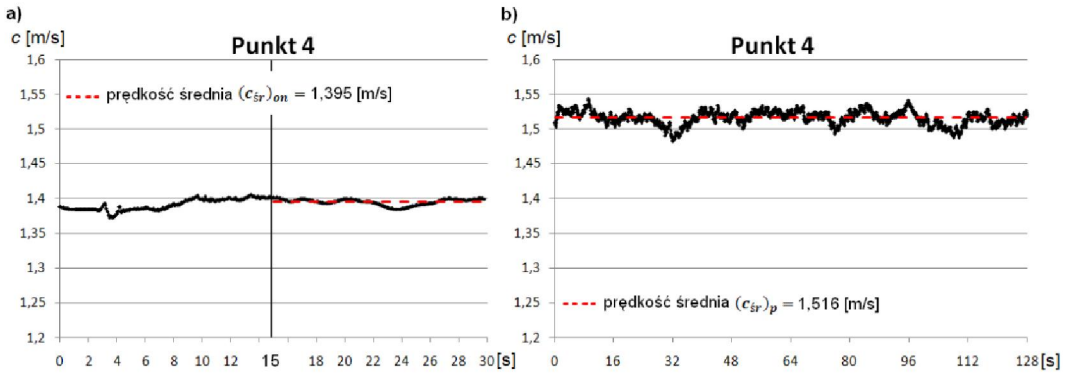

Fig. 30. Time variations of the velocity for the measurement point of the probe 4: a) computed numerically b) measuring the Pitot probe

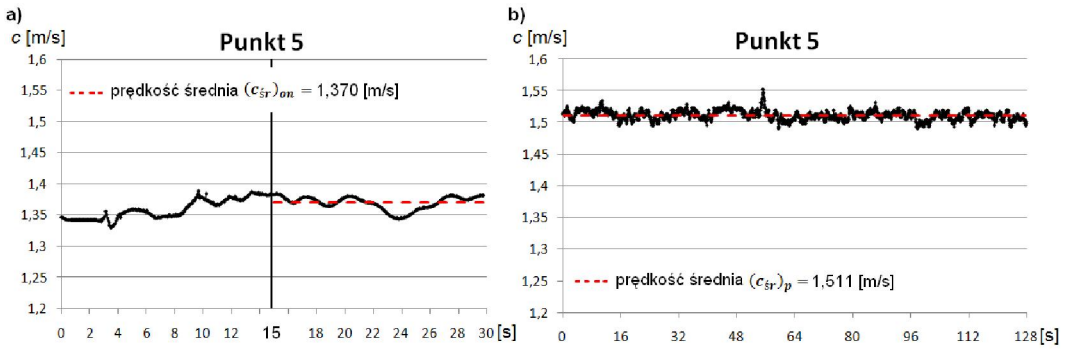

Fig. 31. Time variations of the velocity for the measurement point of the probe 5: a) computed numerically b) measuring the Pitot probe

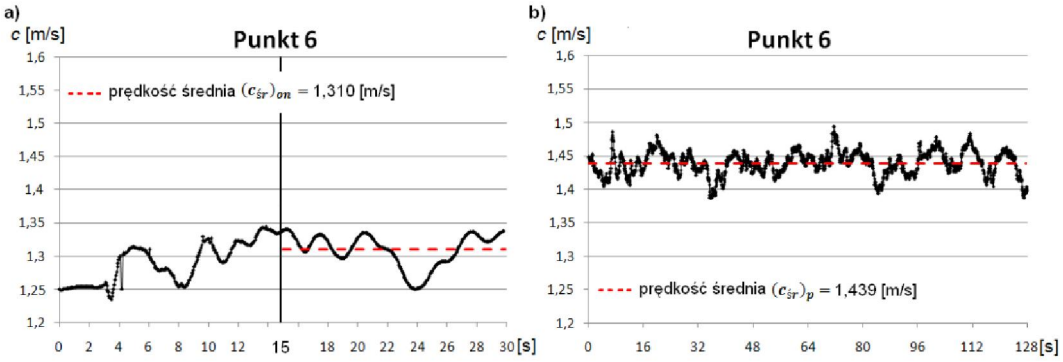

Fig. 32. Time variations of the velocity for the measurement point of the probe 6: a) computed numerically b) measuring the Pitot probe

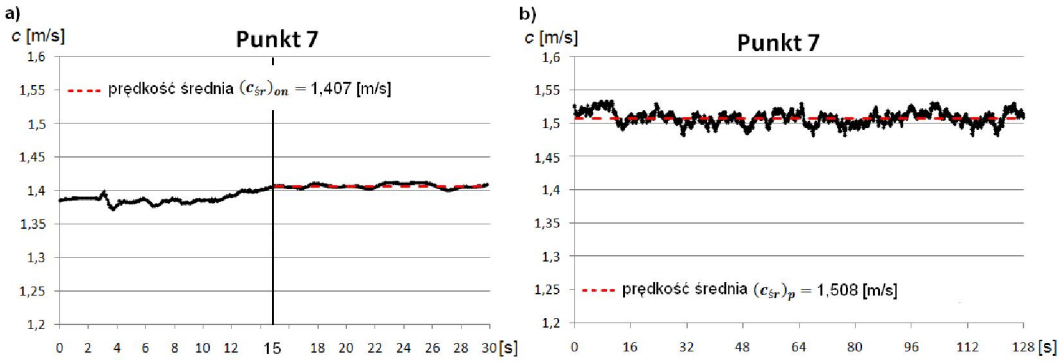

Fig.33. Time variations of the velocity for the measurement point of the probe 7: a) computed numerically b) measuring the Pitot probe

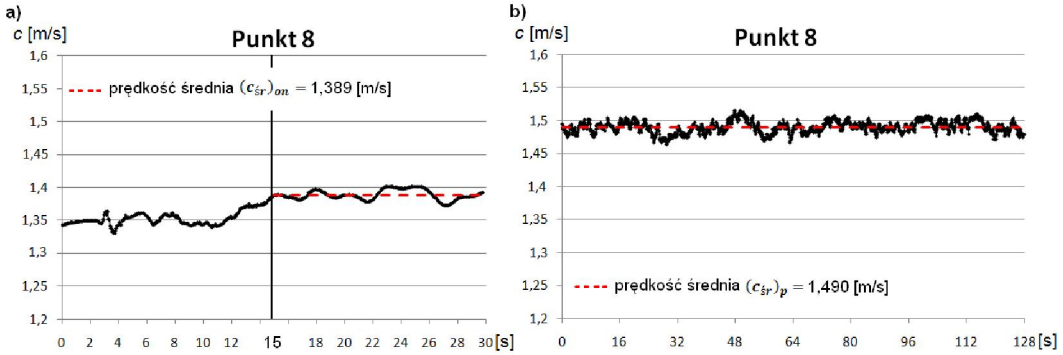

Fig. 34. Time variations of the velocity for the measurement point of the probe 8: a) computed numerically b) using the Pitot probe

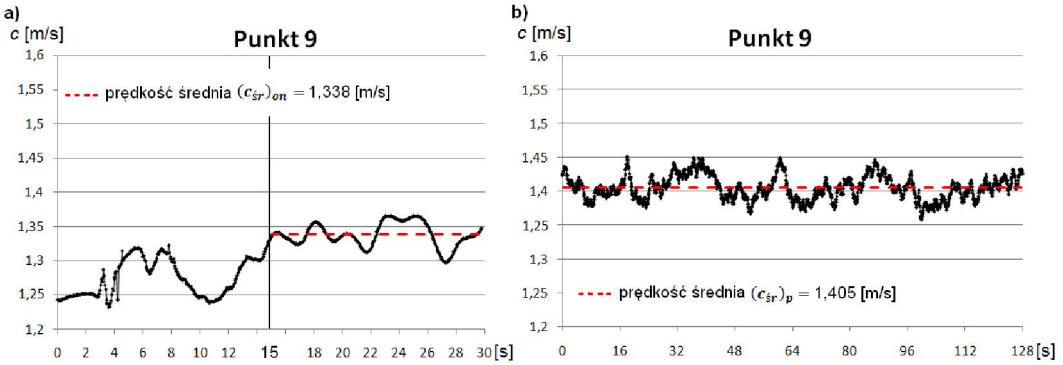

Fig.35 Time variations of the velocity for the measurement point of the probe 9: a) computed numerically b) measuring the Pitot probe

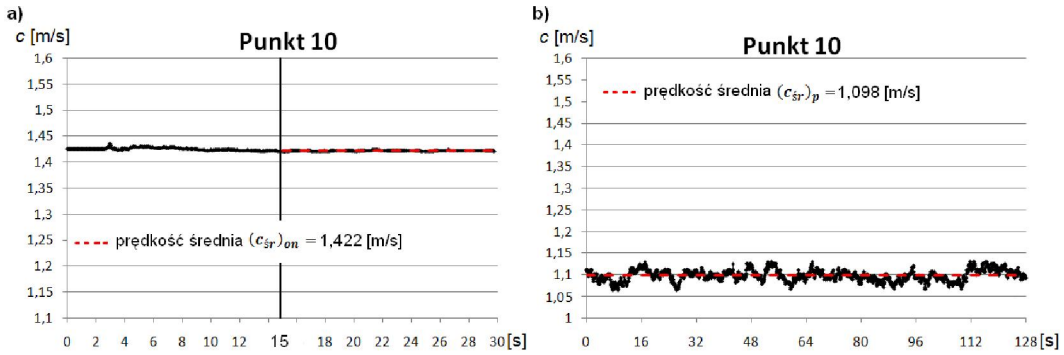

Fig.36. Time variations of the velocity for the measurement point of the probe 10: a) computed numerically b) measuring the Pitot probe

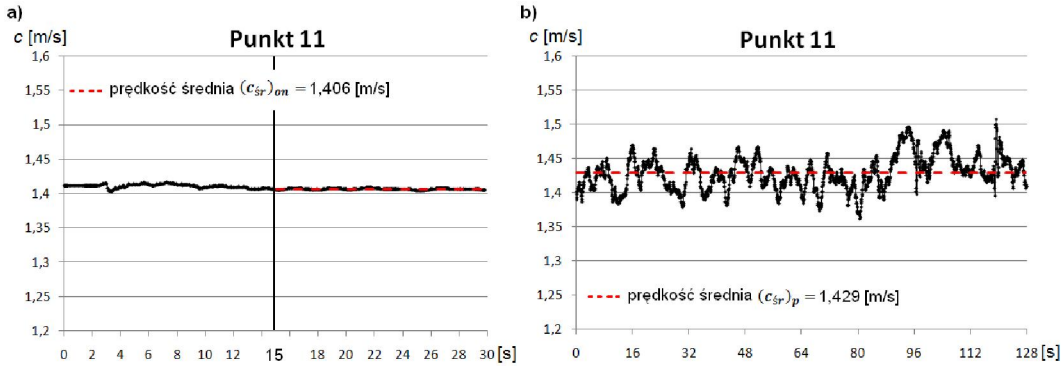

Fig.37. Time variations of the velocity for the measurement point of the probe 11: a) computed numerically b) measuring the Pitot probe

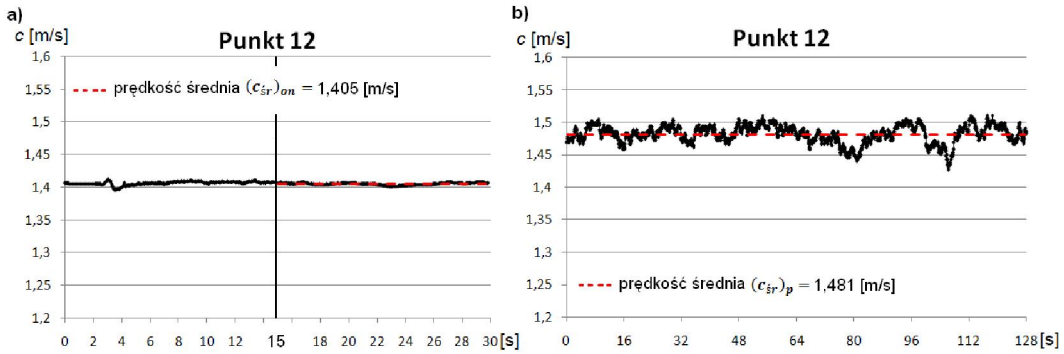

Fig.38. Time variations of the velocity for the measurement point of the probe 12: a) computed numerically b) using the Pitot probe

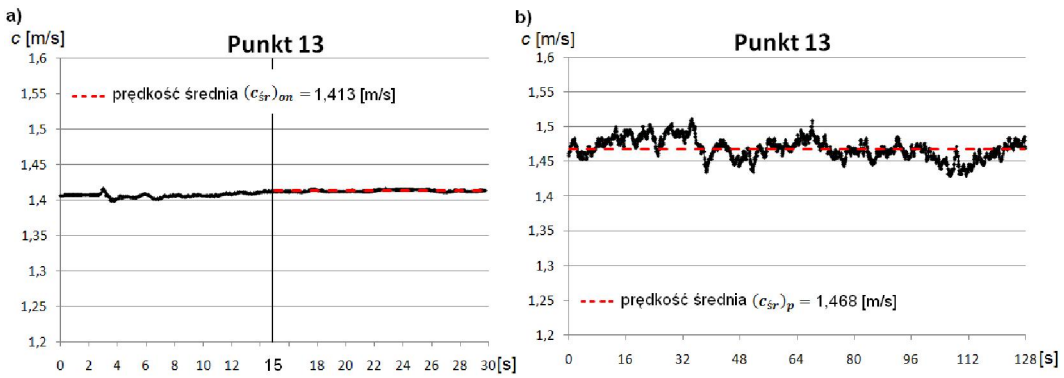

Fig.39. Time variations of the velocity for the measurement point of the probe 13: a) computed numerically b) measuring the Pitot probe

5. Concluding remarks

Results of numerical computations od velocities and velocities from measurements were set together in tables for the suction intake:
- without the rib table T-1 ,T- 2 ,T-3a, T-3b,T-4,
- with the rib T-5, T-6, T-7a, T-7b, T-8.

Computations and measurements were carried-out for the same inflow conditions to the suction intake H_{nom}, Q_{nom}.
In the table T-1 were introduced averaged in time values of velocities from numerical computations and measurements.

Table T-1

measurement points	velocities from numerical computations	velocities from measurements using the pitot probe	relative difference of velocities
	c_{on} $[m/s]$	c_p $[m/s]$	$\frac{c_p - c_{on}}{c_p} \cdot 100\%$
1	1,393	1,433	2,77
2	1,385	1,495	7,37
3	1,365	1,490	8,39
4	1,404	1,494	6,01
5	1,390	1,486	6,44
6	1,351	1,403	3,73
7	1,413	1,486	4,91
8	1,410	1,479	4,68
9	1,387	1,376	-0,81
10	~~1,415~~	~~1,209~~	~~-17,07~~
average	1,389	1,460	4,90

Significant diversification between average velocities from numerical computations and measurements using the probe in point 10 was caused by the wrong location of the probe antenna in the swirl-meter axis trace. Because of this, values of velocities in the point 10 were not considered in computations of average values of velocities.
Maximal relative difference between velocities computed numerically and from measurements is equal to 8,39%. This difference should be considered for acceptable in the aspect of using the proposed computation method of unsteady flows in inlets and suction intakes.
In the table T-2 were set together non-uniformities of the velocity profile from numerical computations and measurements in points of Pitot probe measurements.

Non-uniformity of the velocity profile is defined as the ratio of the time averaged velocity in the given point of the control surface area (there were assumed points of Pitot probe measurements) to average velocity at the surface of the outlet from the suction intake definable from the continuity equation $(c_{śr})_{rc}$.

$$(c_{śr})_{rc} = \frac{4(Q_{\mathrm{nom}})_m}{\pi D_n^2} = 1{,}342\ [\mathrm{m/s}] \qquad (5.1)$$

Where:
Q_n- nominal volume flow,
D_n – diameter of the outlet pipe

Table T-2

1	2	3	4	5	6
Points (Fig. 16)	$(c_{śr})_{rc}$	c_{on}	c_p	Non-uniformities of the velocity profile from numerical computations	Non-uniformities of the velocity profile from measurements
	$[m/s]$	$[m/s]$	$[m/s]$	$\frac{[3]-[2]}{[2]}\cdot 100\%$	$\frac{[4]-[2]}{[2]}\cdot 100\%$
1	1,342	1,393	1,433	3,86	6,82
2	1,342	1,385	1,495	3,23	11,44
3	1,342	1,365	1,49	1,75	11,07
4	1,342	1,404	1,494	4,67	11,37
5	1,342	1,390	1,486	3,64	10,77
6	1,342	1,351	1,403	0,68	4,58
7	1,342	1,413	1,486	5,33	10,77
8	1,342	1,410	1,479	5,09	10,25
9	1,342	1,387	1,376	3,40	2,57
10	~~1,342~~	~~1,415~~	~~1,209~~	~~5,51~~	~~-9,88~~

Distribution of velocity values from measurements and computations has a homothetic character. Higher values of velocities from measurements may be the evidence that thickness of the boundary layer from measurements is higher than defined in numerical computations. In tables T-3a, T-3b were shown adequately amplitudes and velocity fluctuations computed numerically and measured.

Table T-3a

1	2	3	4	5	6	7
Points (Fig. 16)	Amplitudes		$(c_{śr})_{on}$	Relative minimal amplitude	Relative maximal amplitude	Fluctuations $[5]+[6]$
	$(c_{min})_{on}$	$(c_{max})_{on}$		$\frac{[2]-[4]}{[4]}\cdot 100\%$	$\frac{[3]-[4]}{[4]}\cdot 100\%$	
	$[m/s]$	$[m/s]$	$[m/s]$			$[\%]$
1	1,387	1,391	1,389	-0,16	0,13	0,29
2	1,379	1,382	1,381	-0,12	0,10	0,22
3	1,359	1,363	1,361	-0,13	0,16	0,29
4	1,395	1,405	1,400	-0,34	0,38	0,71
5	1,375	1,392	1,384	-0,62	0,61	1,23
6	1,325	1,392	1,343	-1,33	3,66	4,99
7	1,411	1,413	1,412	-0,05	0,09	0,14
8	1,405	1,409	1,407	-0,16	0,13	0,28
9	1,376	1,409	1,380	-0,32	2,07	2,39
10	1,413	1,417	1,415	-0,16	0,12	0,28
11	1,394	1,398	1,396	-0,13	0,16	0,29
12	1,403	1,409	1,406	-0,20	0,23	0,43
13	1,413	1,415	1,414	-0,06	0,08	0,14

Table T3-b

1	2	3	4	5	6	7
Points (Fig. 16)	Amplitudes		$(c_{śr})_p$	Relative minimal amplitude	Relative maximal amplitude	Fluctuations [5] + [6]
	$(c_{min})_p$	$(c_{max})_p$		$\frac{[2]-[4]}{[4]}\cdot 100\%$	$\frac{[3]-[4]}{[4]}\cdot 100\%$	
	$[m/s]$	$[m/s]$	$[m/s]$			[%]
1	1,284	1,533	1,433	-10,40	6,98	17,38
2	1,421	1,564	1,495	-4,95	4,62	9,57
3	1,35	1,556	1,49	-9,40	4,43	13,83
4	1,428	1,574	1,494	-4,42	5,35	9,77
5	1,412	1,546	1,486	-4,98	4,04	9,02
6	1,282	1,519	1,403	-8,62	8,27	16,89
7	1,371	1,55	1,486	-7,74	4,31	12,05
8	1,385	1,59	1,479	-6,36	7,51	13,86
9	1,244	1,51	1,376	-9,59	9,74	19,33
10	1,129	1,282	1,209	-6,62	6,04	12,66

Acceptable by the standard [1] velocity fluctuations were overreached in points 1, 3, 6, 7, 8, 9, 10. Percent values of non-uniformities of the velocity profile in these points were given in the table P T-3b

In the table T-4 were set together velocity fluctuations from numerical computations and measurements and their differences ΔF.

Table T- 1

Points (Fig. 15)		**1**	**2**	**3**	**4**	**5**	**6**	**7**
$(Fluctuations)_p = F_p$	[%]	17,38	9,57	13,83	9,77	9,02	16,89	12,05
$(Fluctuations)_{on} = F_{on}$	[%]	0,29	0,22	0,29	0,71	1,23	4,99	0,14
$\Delta Fluctuations = F_p - F_{on}$	[%]	17,09	9,35	13,54	9,06	7,79	11,9	11,91
Points (Fig. 15)		**8**	**9**	**10**				
$(Fluctuations)_p = F_p$	[%]	13,86	19,33	12,66				
$(Fluctuations)_{on} = F_{on}$	[%]	0,28	2,39	0,28				
$\Delta Fluctuations = F_p - F_{on}$	[%]	13,58	16,94	12,38				

Appearing velocity fluctuations computed numerically and from measurements vary in the scope of 8%÷17%.

In the table T-5 are introduced time averaged velocities from numerical computations and measurements for the suction intake with the rib.

Table T- 2

Measurement points	Velocities from numerical computations	Velocities using the Pitot probe	Relative velocity difference
	$c_{on}\ [m/s]$	$c_p\ [m/s]$	$\frac{c_p - c_{on}}{c_p} \cdot 100\%$
1	1,400	1,484	5,68
2	1,391	1,504	7,53
3	1,369	1,480	7,52
4	1,395	1,516	8,00
5	1,370	1,511	9,34
6	1,310	1,439	8,99
7	1,407	1,508	6,69
8	1,389	1,49	6,79
9	1,338	1,405	4,76
~~10~~	~~1,422~~	~~1,098~~	~~-29,47~~
11	1,406	1,429	1,58
12	1,405	1,481	5,12
13	1,413	1,468	3,76
average	1,383	1,476	6,34

Maximal relative difference between velocities computed numerically and from measurements is 9,34%. This difference is of the same order, as in the variant I. It should be accepted in the aspect of using the proposed method in unsteady flow computations in inlet chambers and suction intakes.
In the table T-6 were set together non-uniformities of the velocity profile from numerical computations and measurements in points of Pitot probe measurement for the suction intake with the rib.

Table T- 3

1	2	3	4	5	6
Points (Fig. 17)	$(c_{śr})_{rc}$	c_{on}	c_p	Non-uniformities of the velocity profile from numerical computations	Non-uniformities of the velocity profile from measurements
	$[m/s]$	$[m/s]$	$[m/s]$	$\frac{[3]-[2]}{[2]} \cdot 100\%$	$\frac{[4]-[2]}{[2]} \cdot 100\%$
1	1,342	1,400	1,484	4,33	10,62
2	1,342	1,391	1,504	3,67	12,11
3	1,342	1,369	1,48	2,03	10,32
4	1,342	1,395	1,516	3,97	13,01
5	1,342	1,370	1,511	2,11	12,63
6	1,342	1,310	1,439	-2,38	7,27
7	1,342	1,407	1,508	4,89	12,41
8	1,342	1,389	1,49	3,53	11,07
9	1,342	1,338	1,405	-0,25	4,73
10	~~1,342~~	~~1,422~~	~~1,098~~	~~5,97~~	~~-18,15~~
11	1,342	1,406	1,429	4,84	6,52

12	1,342	1,405	1,481	4,74	10,40
13	1,342	1,413	1,468	5,31	9,43

In tables T-7a, T-7b were introduced adequately amplitudes and fluctuations of the velocity from measurements for the suction intake with the rib.

Table T- 7a

1	2	3	4	5	6	7
Points (Fig. 17)	Amplitudes		$(c_{śr})_{on}$	Relative minimal amplitude	Relative maximal amplitude	Fluctuations [5] + [6]
	$(c_{min})_{on}$	$(c_{max})_{on}$		$\frac{[2]-[4]}{[4]}\cdot 100\%$	$\frac{[3]-[4]}{[4]}\cdot 100\%$	
	$[m/s]$	$[m/s]$	$[m/s]$			[%]
1	1,397	1,402	1,400	-0,19	0,17	0,36
2	1,388	1,393	1,391	-0,19	0,16	0,36
3	1,367	1,371	1,369	-0,13	0,16	0,29
4	1,384	1,401	1,395	-0,77	0,45	1,22
5	1,344	1,384	1,370	-1,88	1,04	2,92
6	1,25	1,34	1,310	-4,55	2,32	6,87
7	1,401	1,412	1,407	-0,43	0,35	0,78
8	1,372	1,402	1,389	-1,21	0,95	2,16
9	1,297	1,365	1,338	-3,07	2,01	5,08
10	1,42	1,423	1,422	-0,12	0,10	0,21
11	1,404	1,409	1,406	-0,17	0,18	0,36
12	1,401	1,408	1,405	-0,29	0,20	0,50
13	1,411	1,415	1,413	-0,13	0,15	0,28

The highest values velocity amplitudes are in points 6 and 9 located by the outlet pipe wall and are higher than in the case of the suction intake without the rib. They do not exceed values constituted by the standard [1].
In the table T- T-7b were set together non-uniformities of the velocity profile from numerical computations and measurements in points of Pitot probe measurement for the suction intake with the rib.

Table T- 7b

1	2	3	4	5	6	7
Points (Fig. 43)	Amplitudes		$(c_{śr})_{p}$	Relative minimal amplitude	Relative maximal amplitude	Fluctuations [5] + [6]
	$(c_{min})_{p}$	$(c_{max})_{p}$		$\frac{[2]-[4]}{[4]}\cdot 100\%$	$\frac{[3]-[4]}{[4]}\cdot 100\%$	
	$[m/s]$	$[m/s]$	$[m/s]$			[%]
1	1,415	1,586	1,484	-4,65	6,87	11,52
2	1,336	1,675	1,504	-11,17	11,37	22,54
3	1,437	1,534	1,48	-2,91	3,65	6,55
4	1,482	1,544	1,516	-2,24	1,85	4,09
5	1,49	1,552	1,511	-1,39	2,71	4,10

6	1,387	1,493	1,439	-3,61	3,75	7,37
7	1,482	1,534	1,508	-1,72	1,72	3,45
8	1,464	1,516	1,49	-1,74	1,74	3,49
9	1,358	1,451	1,405	-3,35	3,27	6,62
10	1,063	1,131	1,098	-3,19	3,01	6,19
11	1,362	1,508	1,429	-4,69	5,53	10,22
12	1,426	1,511	1,481	-3,71	2,03	5,74
13	1,429	1,511	1,468	-2,66	2,93	5,59

Allowed by the standard [1] fluctuations of the velocity in the suction intake were exceeded in points 1, 2, 11. Measured fluctuations of the velocity in the suction intake with the rib are lower than in the suction intake without the rib. The reason of lower fluctuations in residual points is location of the rib in the suction intake.
In the table T-8 were set together velocity fluctuations from numerical computations and measurements for the suction intake with the rib. Velocity fluctuations from numerical computations and measurements Stage II A.

Table T- 8

Points (Fig. 16)		**1**	**2**	**3**	**4**	**5**	**6**	**7**
$(Fluctuations)_p = F_p$	[%]	11,52	22,54	6,55	4,09	4,10	7,37	3,45
$(Fluctuations)_{on} = F_{on}$	[%]	0,36	0,36	0,29	1,22	2,92	6,87	0,78
$\Delta Fluctuations = F_p - F_{on}$	[%]	11,16	22,18	6,26	2,87	1,18	0,5	2,67
Points (Fig. 16)		**8**	**9**	**10**	**11**	**12**	**13**	
$(Fluctuations)_p = F_p$	[%]	3,49	6,62	6,19	10,22	5,74	5,59	
$(Fluctuations)_{on} = F_{on}$	[%]	2,16	5,08	0,21	0,36	0,5	0,28	
$\Delta Fluctuations = F_p - F_{on}$	[%]	1,33	1,54	5,98	9,86	5,24	5,31	

Occurring differences of fluctuations between these computed numerically and measured using the Pitot probe vary in the scope of 0,5%÷22%.
On the basis of introduced results in tables above, it can be stated that the proposed numerical computation method in unsteady flows is a method which can be used in the design procedure of inlet channels to vertical axial-flow pumps.

REFERENCES

1. American National Standard for Pump Intake Design. ANSI/HI 9.8-1998. Hydraulic Institute. 9 Sylvan Way, Parsippany, New Jersey 07054-3802, www.pumps.org
2. ANSYS CFX, Release 12.1: Theory.
3. Błaszczyk A., Najdecki S., Papierski A., Staniszewski J. Badania modelowe kanału ssącego pompy wody chłodzącej 180P19 na stanowisku nr 8 dla bloku A 460MW w Elektrowni Pątnów. Raport z prac etapu I Arch. IMP PŁ 1542, 2006.
4. Błaszczyk A., Najdecki S., Papierski A., Staniszewski J. Badania modelowe kanału ssącego pompy wody chłodzącej 180P19 na stanowisku nr 8 dla bloku A 460MW w Elektrowni Pątnów. Raport z prac etapu II Arch. IMP PŁ 1546, 2006.
5. Karassik I. J., Messina J. P., Cooper P., Heald Ch. C. Pump Handbook. Third Edition. McGraw-Hill. New York, 2001.
6. Kazimierski Z. Numeryczne wyznaczenie trójwymiarowych przepływów turbulentnych. Maszyny Przepływowe, Łódź 1992, Tom 11.
7. Kuczkowski M. Numeryczny model turbulencji przepływu przez zagięcie przewodu z wykorzystaniem metody LES. Praca doktorska, Łódź 2007.
8. Kunicki R., Numeryczne i doświadczalne badania przepływów nieustalonych w komorach wlotowych pomp. Rozprawa doktorska Łódź 2011.
9. Li S., Lai Y., Weber L., Silva J.M. Patel, V.C. Validation of a 3D Numerical Model for Water Pump Intakes. Journal Hydraulic Research, 42(3), 282-292 - 2004.
10. Mahesh K., Constantinescu S. G., Moin P. A Numerical Method for Large Eddy Simulation in Complex Geometries. Journal of Computational Physics, 197(1), 215-240 - 2004.
11. Menter F.R., Multiscale model fo turbulent flows. 1993, AIAA, 24th Fluid Dynamic Conference.
12. Rajendran V. P., Constantinescu S. G., Patel V. C. Experimental Validation of Numerical Model of Flow in Pump-Intake Bays. Journal of Hydraulic Engineering,125(11), 1119-1125 - 1999.
13. Tullis J.P., Modeling in design of pumping pits. Journal of the Hydraulic Division, Vol. 105, No. HY9, Sept 1979, P. 1053-1063.